Search for Saturn's X-ray aurorae at the arrival of a solar wind shock

G. Branduardi-Raymont,[1] P. G. Ford,[2] K. C. Hansen,[3] L. Lamy,[4] A. Masters,[5] B. Cecconi,[4] A. J. Coates,[1] M. K. Dougherty,[6] G. R. Gladstone,[7] and P. Zarka[4]

Received 8 August 2012; revised 14 December 2012; accepted 31 December 2012; published 22 May 2013.

[1] After a decade of observations, evidence for X-ray auroral emission from Saturn has yet to be found. By analogy with processes known to take place on Jupiter, Saturnian X-ray aurorae may be expected to be powered by charge exchange (CX) between energetic ions and the planet's atmospheric neutrals; if the ions are of solar origin, the emission should be brightest during episodes of enhanced solar wind (SW). We have explored this possibility by propagating SW parameters measured near the Earth to Saturn, and triggering X-ray observations at the time SW enhancements were expected to reach the planet. This was done in April–May 2011 with the Chandra X-ray Observatory, and we report on two observations carried out at the time when a significant SW disturbance reached Saturn, as indicated by Cassini magnetic field, plasma and radio measurements: variability is observed between the two Chandra datasets, but we do not find evidence for X-ray brightening in the auroral regions. The variability can be explained by scattering of solar X-rays in Saturn's atmosphere during an episode of solar X-ray flaring. We conclude that the strength of any CX auroral X-ray emission on Saturn was below Chandra's detectability threshold. By-products of this investigation are stringent upper limits on the X-ray emission of Titan and Enceladus. The Cassini measurements concurrent with the Chandra observations confirm and pinpoint temporally the arrival of the SW enhancement at Saturn. SW propagation predictions are a useful tool for investigating and interpreting the effects of SW interactions with planetary environments.

Citation: Branduardi-Raymont, G., P. G. Ford, K. C. Hansen, L. Lamy, A. Masters, B. Cecconi, A. J. Coates, M. K. Dougherty, G. R. Gladstone, and P. Zarka (2013), Search for Saturn's X-ray aurorae at the arrival of a solar wind shock, *J. Geophys. Res. Space Physics*, *118*, 2145–2156, doi:10.1002/jgra.50112.

1. Introduction

[2] Saturn, like Jupiter, displays powerful auroral emissions at radio, infrared, and UV wavelengths [e.g., *Lamy et al.*, 2010; *Stallard et al.*, 2010; *Clarke et al.*, 2009, and references therein]. However, in contrast with the Jovian case, no X-ray aurorae have been detected for Saturn yet. In this paper, we describe how we set out to search for them with a targeted approach, using solar wind (SW) propagation predictions.

1.1. Saturn's X-rays

[3] Saturn's X-ray emission has been observed several times by Chandra and XMM-Newton over the years 2002–2005 [*Ness et al.*, 2004a, 2004b; *Bhardwaj et al.*, 2005a, 2005b; *Branduardi-Raymont et al.*, 2010, *BR10* hereafter]. The X-ray emission of the planetary disk has a smooth appearance, and its spectrum is well fitted by an optically thin coronal model with an average temperature of ~0.6 keV [*BR10*]. In addition, X-ray emission in the form of a fluorescent oxygen emission line at ~0.53 keV is detected from a "hot spot" on the Eastern ansa of Saturn's rings [*Bhardwaj et al.*, 2005b]. The disk coronal component is generally interpreted as emission produced by the scattering of solar X-rays in Saturn's upper atmosphere, which implies that the disk emission is directly controlled by the Sun [*Bhardwaj et al.*, 2005a].

[4] The strength of the disk X-ray emission is seen to decrease over the period 2002–2005, following the decay of solar activity [*BR10*] toward the extended minimum in the solar cycle from which the Sun is now emerging. The oxygen

[1]Mullard Space Science Laboratory, University College London, Dorking, Surrey, UK.
[2]Massachusetts Institute of Technology, Kavli Institute for Astrophysics and Space Research, Cambridge, Massachusetts, USA.
[3]Department of Atmospheric, Oceanic and Space Sciences, University of Michigan, Ann Arbor, Michigan, USA.
[4]LESIA, Observatoire de Paris, CNRS, UPMC, Université Paris 6, Université Paris Diderot, Meudon, France.
[5]Institute of Space and Astronautical Science, Japan Aerospace Exploration Agency, Kanagawa, Japan.
[6]Space and Atmospheric Physics, Blackett Laboratory, Imperial College London, London, UK.
[7]Southwest Research Institute, San Antonio, Texas, USA.

Corresponding author: G. Branduardi-Raymont, Mullard Space Science Laboratory, University College London, Holmbury St Mary, Dorking, Surrey, RH5 6NT, UK. (g.branduardi-raymont@ucl.ac.uk)

2169-9380/13/10.1002/jgra.50112

line from the rings has also been interpreted as due to scattering of solar X-rays, in this case, by the particles of H_2O ice that are thought to make up the rings [*Bhardwaj et al*., 2005b]. However, by comparing the relative strengths of the disk emission and the oxygen line, it appears that the disk flux does not vary over the years as the line flux does. An alternative possibility for the origin of the X-ray line relates to electron beams injected by Saturnian thunderstorms [*Fischer et al*., 2008], which may excite the ring particles, subsequently producing the fluorescent oxygen line [*BR10*]. In addition to all this, there could be the expectation that, similarly to Jupiter's case [*Branduardi-Raymont et al*., 2007], Saturn may exhibit auroral X-ray emissions produced (below ~2 keV) by the charge exchange (CX) process between energetic ions and atmospheric neutrals, as well as by bremsstrahlung of energetic precipitating electrons (at higher energies). The correlation of UV and radio brightenings of the aurora with the arrival of SW shocks at Saturn [*Clarke et al*., 2009] indicates that SW variability has an impact on auroral processes at this planet; thus, SW ions could be implicated in the CX process (at variance with Jupiter where spectral fits suggest that CX emission is due to highly accelerated precipitating ions of magnetospheric origin [*Hui et al*., 2010a]).

1.2. X-rays by Solar Wind Charge Exchange

[5] CX between highly ionized ions and neutrals is a particularly effective mechanism for producing soft X-rays: the process involves the collision of a highly ionized ion with a neutral atom or molecule, the subsequent acquisition of an electron by the ion, and then the emission of a characteristic X-ray line following the ion's de-excitation. The significance of CX in generating X-rays, though, was recognized only about 15 years ago [*Cravens*, 1997], following the discovery that comets are strong soft X-ray sources. In this case, the process is particularly efficient because of the extensive coma of neutrals surrounding cometary nuclei, which travel within the ion-rich SW; hence the name "solar wind charge exchange" or SWCX (see the comprehensive review by *Dennerl* [2010] and references therein).

[6] The X-ray power produced per unit volume by SWCX, assuming only one CX collision per SW ion, depends linearly on the density of neutrals n, on the SW density n_{SW}, and on the SW speed v_{SW} [*Cravens*, 2000]:

$$P_X = \alpha \; n \quad n_{SW} v_{SW} \quad \text{eV cm}^{-3}\text{s}^{-1} \tag{1}$$

where the proportionality parameter α incorporates all the atomic physics details (e.g., cross sections) and SW ion abundances and is estimated to be between 6×10^{-16} and 6×10^{-15} eV cm^2[*Cravens*, 2000, and references therein].

[7] The ionization state of the SW is also an important parameter for the generation of SWCX X-rays: for example, *Bodewits et al*. [2007] demonstrated that cometary X-ray spectra mainly reflect the state of the local SW; this is further supported by the extreme X-ray faintness of comet 17P/Holmes which was exposed to the high latitude SW, known to be depleted of highly charged ions [*Christian et al*., 2010].

1.3. Solar Wind–auroral Activity Connections

[8] Saturnian X-ray aurorae may have gone undetected so far if they generally lay below the sensitivity threshold of current Earth-bound X-ray observatories. However, if they are produced by the CX process, we can expect to maximize the chances of detecting them by choosing to observe at a time when episodes of enhanced SW density and speed reach Saturn. This approach is supported by the results of *Prangé et al*. [2004] in the case of a series of coronal mass ejections (CMEs) propagating to Jupiter and then to Saturn in November to December 2000, at a time when both planets were close to opposition. The shocks associated with the CMEs were understood, a posteriori, to have taken about a month to reach Saturn, where they are believed to have been responsible for a very unusual FUV auroral display. On their way to Saturn, the shocks were found to have caused FUV auroral storms on Earth and to have enhanced auroral radio activity on Jupiter.

[9] The relationship between auroral brightenings at Saturn and solar wind compressions was clearly demonstrated by *Clarke et al*. [2005]. More recently, following a large-scale coordinated campaign of HST observations and Cassini in situ measurements at Saturn, complemented by propagation predictions of SW conditions from 1 AU to near the outer planets, *Clarke et al*. [2009] were able to associate brightenings of both Saturn's UV auroral emissions and its kilometric radiation with the arrival of SW shocks and pressure increases; they concluded that this behavior is consistent with a causal relationship between the two events. Both *Prangé et al*. [2004] and *Clarke et al*. [2009] noted that the correlation at Jupiter is weaker than that at Saturn, which may reflect the fact that the Jovian auroral activity is controlled by factors intrinsic to the planet and its immediate environment rather than by the SW. However, magnetospheric compression may well play a role also in the Jupiter case: strong flux and spectral variability in the auroral X-ray emission above 2 keV (due to electron bremsstrahlung) was observed at the time of the arrival at the planet of the "Halloween storm" in November 2003 [*Branduardi-Raymont et al*., 2007].

[10] In this article, we describe how we have attempted to go further in this approach, i.e., by exploiting the assumption that the passage of SW shocks can energize aurorae at the outer planets, by trying to predict in advance when a disturbance would reach Saturn, and then triggering a Chandra observation, in search of X-ray aurorae, to coincide with its arrival at the planet. A similar strategy has led recently to the successful detection with the Hubble Space Telescope of UV aurorae on Uranus [*Lamy et al*., 2012]. Here we try to adopt such a "predictive strategy" in the X-ray band, by propagating a SW shock from its observation at 1 AU to an outer planet; applying this approach in another energy band is relevant because different physical processes, in some cases operating on the same population of charged particles, are responsible for the spectrum of the aurorae: for example, SKR emissions can only be triggered by electrons, which also produce UV emission and the >2 keV X-ray bremsstrahlung.

[11] Theoretical estimates of expected CX auroral fluxes from Saturn due to unaccelerated precipitating SW ions have been presented by *Hui et al*. [2010b], assuming the whole polar cap as the emission area. These are within a factor of a few of the sensitivity we can expect with Chandra; field-aligned acceleration of SW ions would raise these estimates but cannot involve >100 kV potentials not to exceed the

current X-ray upper limits [*Hui et al*., 2010b]. The likelihood of detecting X-ray bremsstrahlung from Saturn's aurora is lower, scaling from what is known for Jupiter [*Branduardi-Raymont et al*., 2007]. In section 5.1, we make a detailed comparison of our results with theoretical expectations.

[12] We have used the 1-D MHD code mSWiM [*Zieger and Hansen*, 2008, http://mswim.engin.umich.edu] to propagate SW parameters from 1 AU to the outer planets. The details of our predictive strategy are described in the next section. Sections 3 and 4 describe the Chandra X-ray observations and the contemporaneous Cassini in situ SW and remote radio measurements, respectively; we discuss our results in section 5 and summarize our conclusions in section 6.

2. Propagation Predictions

[13] In early 2011, the Sun appeared to begin to emerge from an extended minimum in its activity cycle, producing significant Earth-bound CMEs and > C flares in mid February and March 2011 (e.g., see http://secchi.nrl.navy.mil/cactus/). This was the signal we had been waiting for, hoping we could trigger Chandra Target of Opportunity (TOO) observations to coincide with the arrival of a disturbance at Saturn.

[14] We used the mSWiM code to predict the SW propagation from Earth to Saturn, basing the calculations on ACE and WIND velocity and density SW data extracted from the OmniWeb database. The code uses SW parameters at Earth going back several months so that their cumulative effects are taken into account and predicts their values at later times of arrival at the outer planets. SW speed is generally the most accurately propagated parameter, and density predictions are more reliable when close to opposition. On the basis of extensive statistical validation work using the average observed timing error for a number of SW shocks [*Zieger and Hansen*, 2008], predictions are expected to be most accurate for times within ±75 days of the planet's opposition, one of which occurred for Saturn on 4 April 2011. The highest accuracy is attained during years of solar activity high recurrence index, usually corresponding to the declining phase of the solar cycle; around the maximum of solar activity, the model predicts shocks arriving later than observed with in situ data. While a detailed discussion of the propagations timing accuracy is beyond the scope of this paper (and is presented in *Zieger and Hansen* [2008]), we note that *Clarke et al*. [2009] found significant shifts between the arrival of propagated SW shocks and their in situ detections at Jupiter (+2.1 days during the New Horizons fly-by in February to March 2007) and at Saturn (+2.6 days, measured by Cassini in February 2008). As described in section 1.2, the SWCX X-ray emission power depends linearly on SW density and speed; the mSWiM code predicted that a strong enhancement in these SW parameters would occur at Saturn in late April to early May 2011 (see Figure 1); this was deemed to be a good case for triggering TOO observations of Saturn with Chandra. Two observations of 80 ks, separated by approximately 1 day, were planned (red segments in the bottom panel of Figure 1) in the attempt of covering a ~2 day period of uncertainty in the arrival time of the SW disturbance at Saturn and to search for variability in the planet's X-ray emission, which may reflect changes in SW conditions.

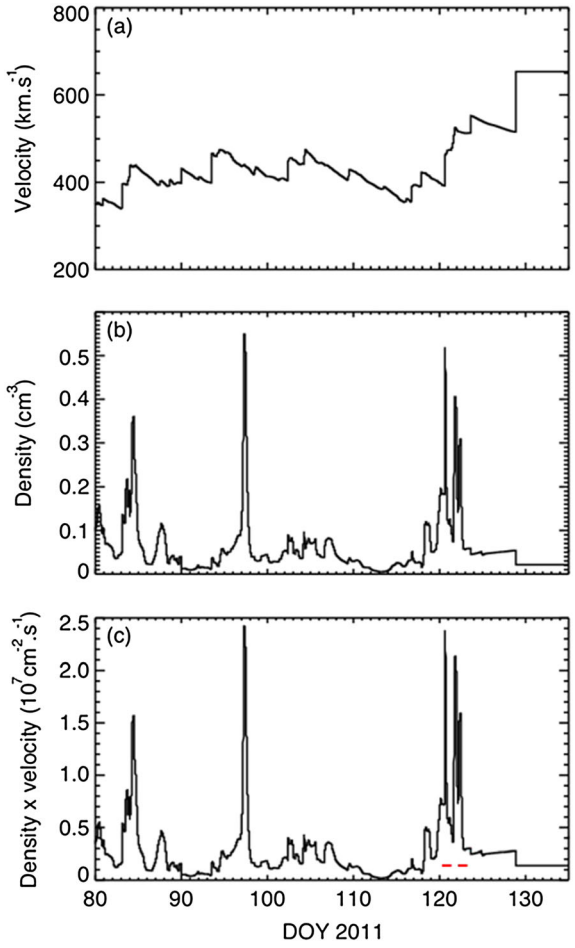

Figure 1. Results of the propagation to Saturn of SW parameters at 1 AU from OmniWeb data covering the period up to day of year (DOY) 130 of 2011. Predicted SW velocity and density values at Saturn (top and middle panels) and the product of the two (i.e., the SW number flux; bottom panel) show that a large enhancement was expected to arrive at Saturn around DOY 120 (30 April 2011). The two red segments in the bottom panel mark the times of the Chandra observations.

3. Chandra X-ray Observations

[15] Two Chandra ACIS observations of 80 ks each were carried out starting on 30 April, 05:48 UT, and on 2 May, 08:30 UT, when the planet was at a distance of 8.7 AU from Earth and 9.6 AU from the Sun, and its disk had an apparent diameter of 19 arcsec. X-rays from Saturn were clearly detected on both occasions, and variability was found to have occurred between the two datasets.

[16] At the beginning of each of the two ACIS-S observations (obsids 12317 and 12318), Saturn was positioned in the field of view (FOV) of the S3 CCD chip so that its equatorial plane (at ~ 3° from its direction of proper motion) was imaged out to ~30 Saturn radii for the full observing time; this was done to cover the locations of its satellites, Enceladus in particular. Following the recent Cassini detection of magnetic

field–aligned ion and electron beams downstream from Enceladus and the subsequent discovery of Enceladus-associated auroral footprints by Cassini/UVIS [*Pryor et al*., 2011], we intended to search for X-ray emission from both Enceladus (at 3.9 R_S) and Titan (20.3 R_S). The optical brightness of Saturn is sufficiently low that no special observing mode was needed to reject the near-IR light leak in the ACIS-S optical blocking filter (OBF); Saturn was kept out of the FOV during bias map accumulations, and corner pixels were used in the analysis to calculate CCD threshold levels [*Ford and Elsner*, 2005].

[17] In the subsequent data analysis, first, X-rays from background sources in the field were removed, and the remaining X-ray events were reprojected into Saturn-fixed coordinates, to remove the planet's proper motion; after correcting for image dither and possible red light leak through the OBF, images and spectra of Saturn were constructed, as well as ACIS response matrices, using the standard CIAO software and the most recent Chandra calibration database. Compared with previous ACIS observations of Saturn, there was little indication of a light leak in the corner pixels of 5 × 5 event "islands," probably because the ring plane angle was much larger during the 2003 and 2004 observations so that the rings then made a much larger contribution to the optical signal. The data were processed both with and without the light leak correction procedure, without any significant difference. All results reported here were obtained with the corrected dataset.

3.1. Images and Light Curves

[18] Figure 2 shows the ACIS images of Saturn obtained from the two 2011 observations separated by a 1 day gap. The images (in the bands 0.3–2.0 keV, top, and 0.49–0.62 keV, bottom) have been smoothed with a Gaussian filter of σ equal to 0.492 arcsec; the green circles and ellipses show the extent of Saturn's disk and of its A, B, and C rings.

[19] Table 1 lists gross and net counts (and errors) for Saturn's disk (excluding the area obscured by the rings, thus the heading "Disk overlapping rings"), for the parts of the disk of equal area above and below the larger ellipse outlining the rings (named North and South caps) and for the parts of the rings away from the disk (East and West ansae). Net counts are after subtraction of the background (also listed in Table 1), estimated from source-free regions several times larger than the planet; this is an upper limit to the true background level

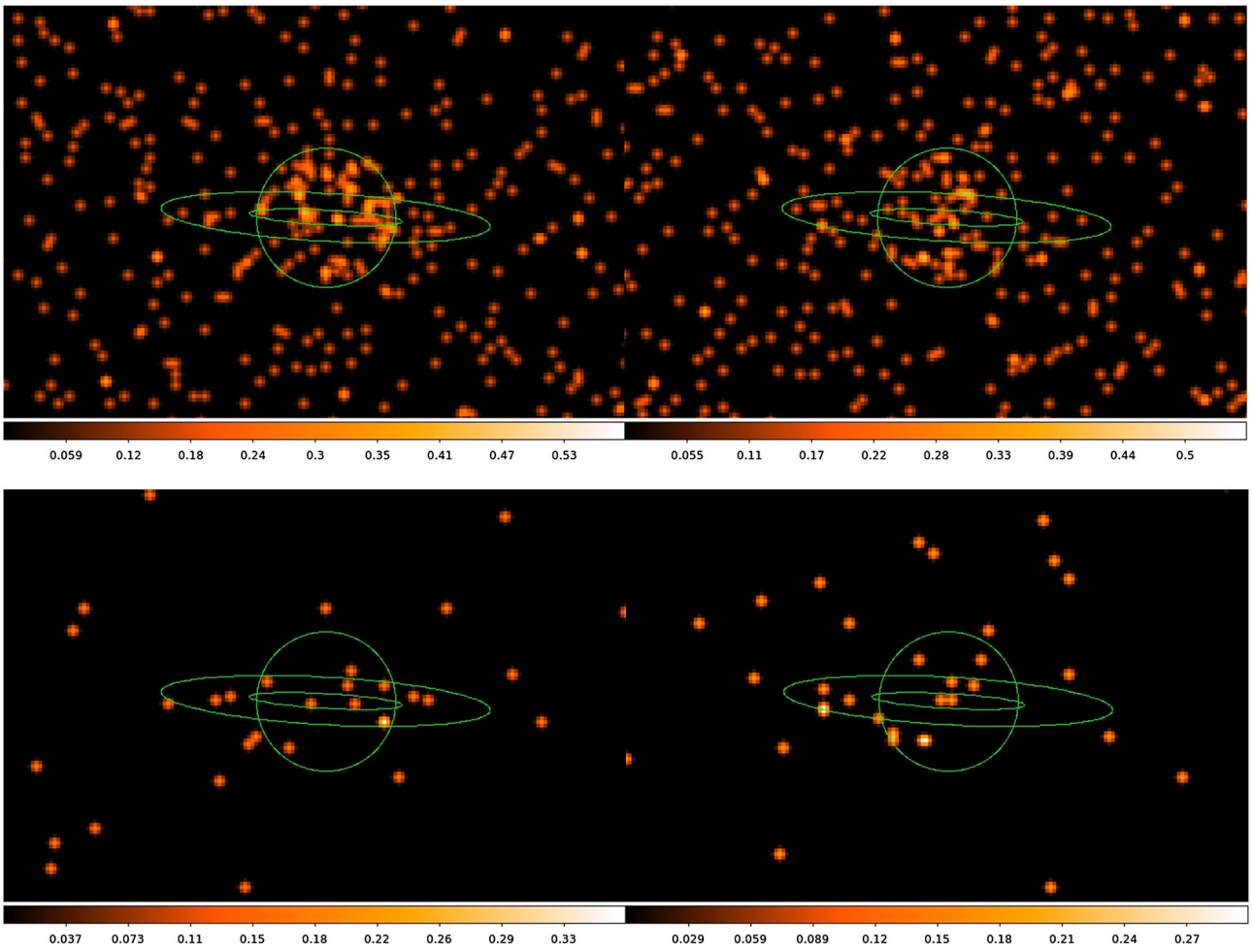

Figure 2. Chandra ACIS images of Saturn in the bands 0.3–2.0 keV (top) and 0.49–0.62 keV (bottom) from observations on 30 April (left) and 2 May 2011 (right). The data have been smoothed with a Gaussian filter of σ equal to 1 pixel (or 0.492"). The green circles are centered on the planet and have radii of 9.5" (equal to Saturn's apparent radius at the time); the larger ellipse has a major axis of 45", which corresponds to the full extent of the A, B, and C rings. The color scale is in counts/pixel.

Table 1. Counts Extracted From the Chandra ACIS Images of Saturn

	0.3–2.0 keV	0.3–2.0 keV	0.3–2.0 keV	0.3–2.0 keV	0.49–0.62 keV	0.49–0.62 keV	0.49–0.62 keV	0.49–0.62 keV
Saturn counts	gross counts	net counts	error	b/g expected	gross counts	net counts	error	b/g expected
Chandra 30 April 2011								
Disk-overlapping rings	65	52.2	8.1	12.8	5	3.9	2.2	1.1
North cap	29	24.3	5.4	4.7	1	0.6	1.0	0.4
South cap	15	10.3	3.9	4.7	1	0.0		0.4
East ansa	6	2.8	2.5	3.2	2	1.7	1.4	0.3
West ansa	8	4.8	2.8	3.2	2	1.7	1.4	0.3
Chandra 2 May 2011								
Disk-overlapping rings	51	36.9	7.2	14.1	10	8.6	3.2	1.4
North cap	19	13.8	4.4	5.2	2	1.5	1.4	0.5
South cap	20	14.8	4.5	5.2	4	3.5	2.0	0.5
East ansa	8	4.5	2.8	3.5	3	2.7	1.7	0.3
West ansa	4	0.0		3.5	0	0.0		0.3

since Saturn is a foreground target. In the 0.3–2.0 keV band, the planet's disk brightness decreases by 30^{+20}_{-30}% between the first and the second observation. While there is no visible enhancement in the emission at the poles, the North cap is more than twice as bright as the South in the first observation; however, they are of comparable brightness in the second. Some 0.3–2.0 keV flux is present in the ring ansae above the background level. There is also excess flux in the ansae in the 0.49–0.62 keV band, where the O line lies, except for the West ansa in the second observation; however, the statistical probability of observing two or three events when 0.3 are expected is rather high (3×10^{-2} and 3×10^{-3}, respectively).

[20] There is typically only one 0.3–2.0 keV event in each of the auroral regions extending 20° down from the North and South pole, respectively (Figure 2); by combining the two observations, we obtain a 3σ upper limit of 2.7×10^{-5} count s^{-1} for any CX auroral X-rays that may be present in addition to the disk emission. A very similar number of events, and thus the same upper limit, apply in the range 2.0–8.0 keV.

[21] Saturn's disk X-ray light curves within the individual observations were searched for variability; however, nothing significant was found, and folding them on the planet's 38 ks equatorial rotation period does not reveal any enhancement at that period.

3.2. Spectral Analysis

[22] Spectra of Saturn's disk were extracted from a circle with a radius of 19 ACIS pixels (equivalent to 9.5 arcsec, the planet's apparent equatorial radius) centered on the planet, excluding the area covered by the rings (i.e., the area between the two ellipses lying in front of the planet's disk; see Figure 2); the background was extracted from an annulus concentric with the planet, of inner and outer radii of 30 and 200 pixels (15 and 100 arcsec), respectively. The spectra were modeled over the 0.3–2.0 kev band using the XSPEC v. 12.6.0 fitting code. The spectrum from the first observation, when Saturn's disk was brighter, is well described by an optically thin, coronal model (`mekal` component in XSPEC) and a Gaussian emission line at 1.38 keV, consistent within the errors with the energy of the Mg XI triplet transition at 1.35 keV. We tested the significance of this line by refitting the spectrum without including it in the model; the total χ^2 rises from 1.0 to 5.3 for two additional degrees of freedom, with all the increase being due to excess flux in the highest energy bin (where the line lies). The spectrum from the second observation, when Saturn's disk was dimmer, is adequately fitted by a `mekal` component and an emission line of energy fixed at 1.35 keV (although the flux in this line is consistent with zero within the errors). Table 2 lists exposure times, total number of source net counts in the spectra, best fit parameters with 90% confidence errors, energy fluxes for the two observations (individually and combined), and the two spectral components separately; the corresponding emitted powers for the full disk of Saturn (i.e., after correcting for the ring-occulted part) are also included: the conversion from flux to power has

Table 2. Best Fitting Results for the Chandra ACIS Spectra of Saturn (errors are at 90% confidence)

Observation Start Time	Total Exposure Time (ks)	Saturn Net Counts	`Mekal` kT (keV)	`Mekal` norm[a]	`Mekal` flux[b]	`Mekal` power (MW)[c]	Gauss energy (keV)	Gauss norm[d]	Gauss flux[e]	Gauss power (MW)[c]	χ^2/ dof
30 April 2011, 05:48 UT	78	53	0.49 +0.14 –0.13	0.93 +0.21 –0.32	2.4	64	1.38 +0.33 –0.31	0.15 +0.21 –0.12	0.4	11	0.97/2
2 May 2011, 08:30 UT	79	40	0.37 +0.19 –0.09	0.75 +0.33 –0.30	1.9	50	1.35 fixed	0.1 +0.1 –0.1	0.2	5	1.24/2
Both observations combined	158	105	0.47 +0.12 –0.12	0.73 +0.24 –0.17	2.0	53	1.39 +0.04 –0.16	0.12 +0.07 –0.08	0.3	8	1.59/8

[a] `Mekal` normalization at 1 keV in units of 10^{-6} ph cm^{-2} s^{-1} keV^{-1}.
[b] Total 0.3–2.0 keV energy flux in the `mekal` component in units of 10^{-18} W m^{-2}.
[c] Normalized to full disk (multiplying by 1.25).
[d] Gaussian line normalization in units of 10^{-6} ph cm^{-2} s^{-1}.
[e] Total energy flux in the line in units of 10^{-18} W m^{-2}.

been made by multiplying the flux values by $4\pi d^2$, where d is the geocentric distance of Saturn at the time, i.e., 8.7 AU.

[23] The 0.3–2.0 keV 3σ countrate upper limit on any CX auroral emission (see sec. 3.1) is equivalent to an energy flux of 0.1×10^{-18} W m^{-2} for the disk best fit `mekal` model, which is a reasonable average approximation for a line-rich CX spectrum. These fluxes correspond to a power upper limit for the CX emission of 2.1 MW. The 3σ upper limit on the 2.0–8.0 keV countrate is equivalent to a flux of 0.8×10^{-18} W m^{-2} and to an emitted power of 17 MW, for a bremsstrahlung model with kT = 10 keV.

[24] Figure 3 shows the ACIS spectra and the best fits for Saturn's disk for the two 2011 observations separately and combined.

[25] Spectra for the ansae of Saturn's rings were also extracted and combined for each observation, and then, both observations were combined. While the low number of counts prohibits formal spectral fitting, visual inspection of the background-subtracted spectra (Figure 4) reveals the clear presence of an emission line with energy consistent with that (0.53 keV) of a fluorescent OKα line. From the number of 0.49–0.62 keV events left after background subtraction, taking a Chandra ACIS effective area of 120 cm^2 at 0.5 keV, we derive energy fluxes of 0.31 and 0.24×10^{-18} W m^{-2}, corresponding to emitted powers of $7^{+}_{-}4$ and $5^{+}_{-}3$ MW for the first and second observation, respectively.

3.3. Search for X-rays From Saturn's Satellites

[26] The X-ray events detected during the Chandra observations were re-registered in the coordinate reference systems of Saturn's satellites Titan and Enceladus. After subtracting X-rays originating from Saturn and its rings, no significant enhancements in X-ray flux were found at the moon locations: within a circle of 5 arcsec radius (encircling 100% of the ACIS Point Response Function), we expect an average background level of ~ 4 counts over the duration of each observation, which implies a combined 3σ upper limit of 5.4×10^{-5} count s^{-1} (~4 MW for Saturn's disk `mekal` best fit model; see section 3.2) for both Titan and Enceladus.

4. Cassini Measurements

4.1. Cassini Boundary Crossings

[27] During an interval that included the Chandra observations, Cassini made crossings of Saturn's magnetopause and bow shock. We have identified these crossings, and we have compared them to the SW parameters propagated with the mSWiM code (see section 2). Our aim is to correlate a distinct feature in the set of Cassini boundary crossings with a feature in the SW propagations. By doing this, we can estimate the time shift that needs to be applied to the propagations, making them a very powerful tool for examining the history of magnetospheric expansion/compression episodes around this time, and thus, the effect that they may have on X-ray auroral production on Saturn.

[28] We have used Cassini MAG (MAGnetometer, *Dougherty et al.*, 2004) data to establish which regime the spacecraft was in (upstream SW/magnetosheath/magnetosphere; see Figure 5a) and Cassini ELS (ELectron Spectrometer; *Linder et al.*, 1998, *Young et al.*, 2004) spectra to validate this and for boundary identification (Figure 5b). Cassini was inbound at around 17:00 SLT (Saturn local time) on 30 April 2011 (day of year, DOY 120), keeping at low latitude for an extended interval surrounding the Chandra

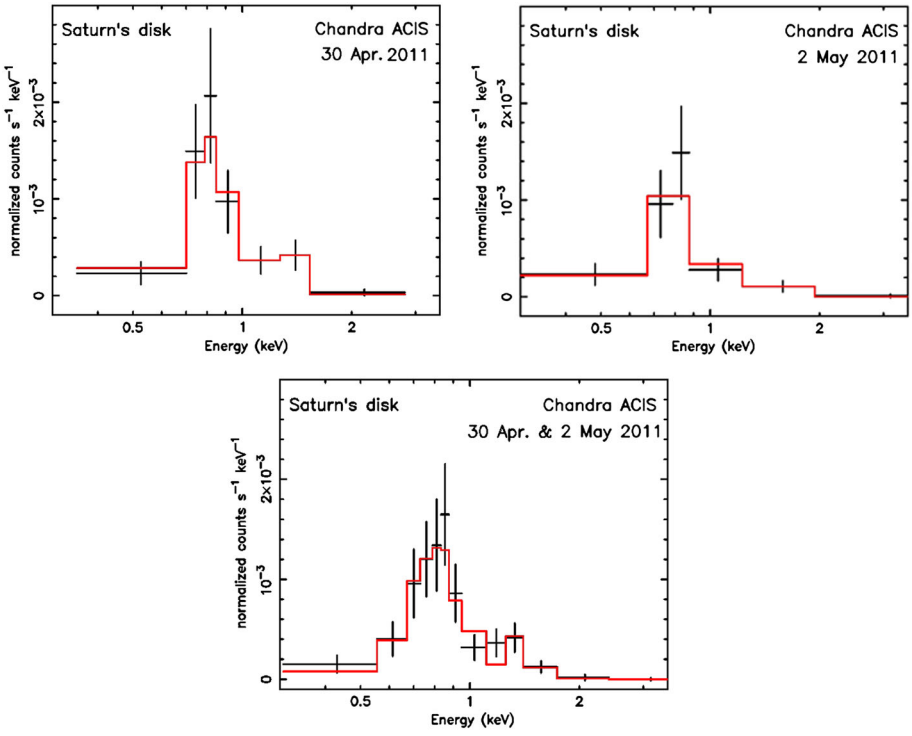

Figure 3. (top) Chandra ACIS spectra of Saturn's disk for the first (left) and second (right) 2011 observation. Data are shown as black crosses and the best fits as red histograms. (bottom) Combined ACIS spectrum for the two observations.

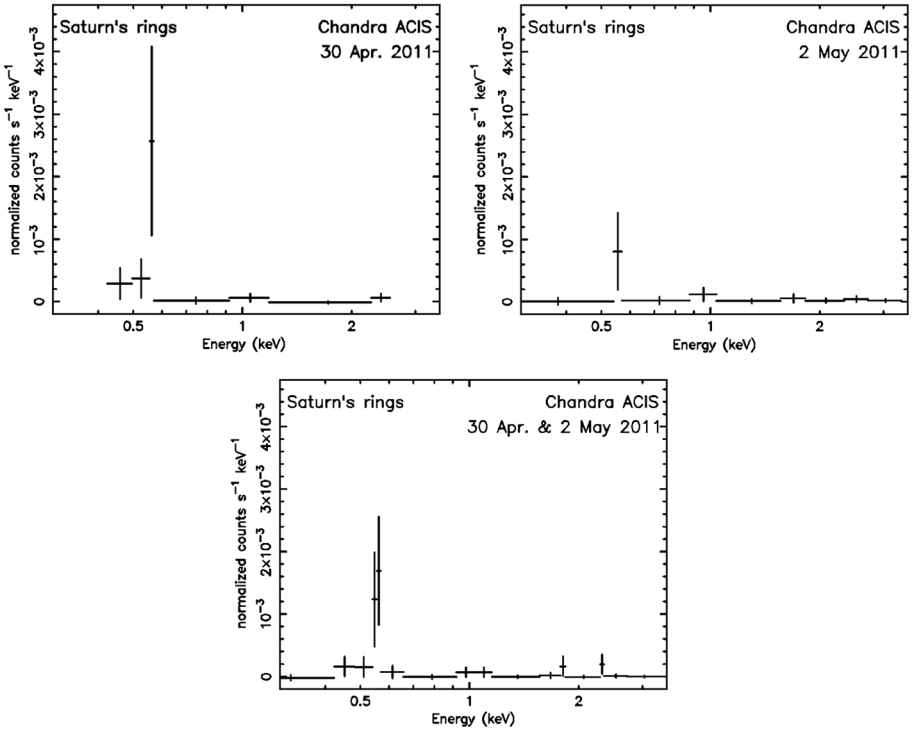

Figure 4. (top) Chandra ACIS spectra of Saturn's rings for the first (left) and second (right) 2011 observation. An emission line at an energy consistent with that (0.53 keV) of the fluorescent OKα line is clearly present (the energy bins are of different size because of the requirement that each contains at least 2 counts). (bottom) Combined ACIS spectrum for the two observations.

observations. A number of bow shock crossings took place over an interval of a few Earth days, followed by magnetopause crossings over less than 1 day.

[29] In the following, we describe how we compared information derived from the crossing times with the propagations. The standoff distances of the boundaries (bow shock and magnetopause), i.e., the distances between the center of Saturn and the boundary of interest along the planet-Sun line, are a proxy for the size of the system. The propagated densities and speeds yield dynamic pressures, which are related to the standoff distances by simple power laws [*Kanani et al.*, 2010, *Went et al.*, 2011]; we can therefore derive the propagated (i.e., predicted) standoff distances of both the bow shock and magnetopause. From these, we can infer the radial distances of the two boundaries along the radial vector through the spacecraft, to predict the regime Cassini should be in. By comparing these radial distances predicted from the propagations with those inferred from the in situ measurements, we can estimate the required time shift to apply to the propagations.

[30] Figures 5c and 5d summarize the Cassini-mSWiM comparison by displaying radial distances versus time. The clearest feature present in both data sets is a rapid expansion of the system before it maintains a steady size for several days at the end of the coverage. However, the shock is observed significantly closer to the planet than the propagations predict. Cassini then sees the bow shock (blue dot) and the magnetopause (red dot) in quick succession on DOY 124. Subsequent magnetopause crossings occur within a few hours, suggesting that the size of the magnetosphere was relatively constant from this time on (in agreement with the propagations, indicated by the blue and red continuous curves, toward the end of the interval). Cassini only stopped crossing the magnetopause because it had got closer to the planet by the end of this extended interval.

[31] Based on this comparison and the trends observed, we have applied a shift of +1.9036 days to the propagations (blue and red continuous curves) to match up these features; the result (Figure 5d) shows a very good qualitative agreement between Cassini and mSWiM in the trend displayed by both datasets, and a good quantitative agreement as well, considering that the uncertainties on the radial distances derived from Cassini are of the order of a few R_S. Note that the last bow shock crossing is followed very closely by a magnetopause crossing. This is clear and unambiguous evidence for magnetospheric expansion, which is captured thanks to the time shift applied to the propagations. To ease comparisons, Figure 5e displays the product of the predicted SW density and velocity values (the so-called "SW number flux") at Saturn (from Figure 1) for the period of interest, after the +1.9 days shift.

[32] The shift of +1.9 days that has to be applied to the propagations in order to match them with the Cassini measurements is significantly longer than the ~0.5 day uncertainty expected in the arrival time of the SW shocks when the planet is close to opposition [*Zieger and Hansen*, 2008] but is consistent in magnitude and direction with those established by *Clarke et al.* [2009] (see sec. 2). This may reflect the fact that their and our observations took place past the declining phase of the solar cycle. Future improvements in the MHD code (such as enhancing it to work in 2-D), as well as further validations like the one

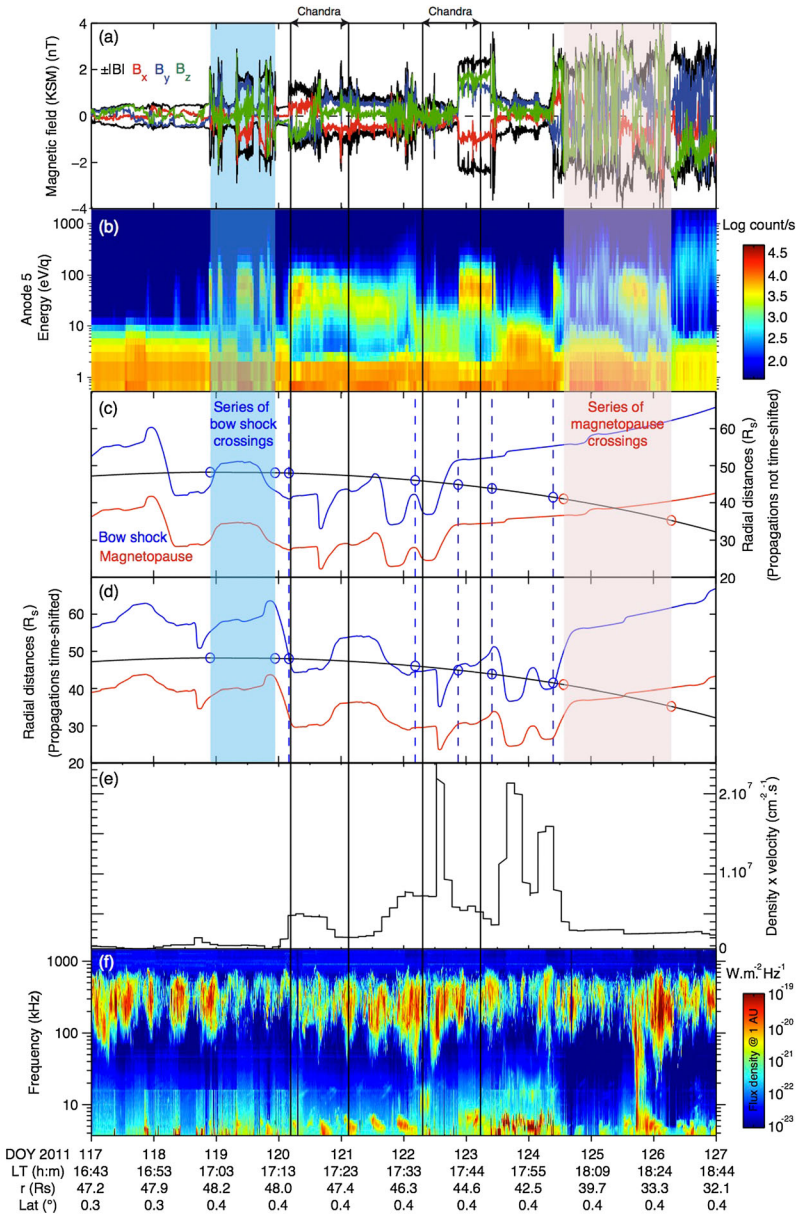

Figure 5. Cassini-mSWiM comparison. Time (UT Cassini for in situ data, delayed by 6 to 10 seconds with respect to UT Saturn) runs along the horizontal axis, as well as Saturn Local Time (LT; the widening intervals between tick marks are due to the spacecraft accelerating with decreasing distance from the planet), Cassini distance r from Saturn (in Saturn radii R_S), and Cassini latitude. (top) The two black segments with arrows show the intervals covered by the Chandra observations, corrected for the light travel time from Saturn to Earth (~1.2 hr). (a) Magnetic field measurements by Cassini MAG in Kronocentric Solar Magnetospheric (KSM) coordinates. (b) Cassini ELS spectrogram. (c) and (d) Plots of radial distances. Blue: Bow shock, Red: Magnetopause. The blue dashed vertical lines give the time of Cassini bow shock crossings (as seen in the MAG data). The black curve shows the radial distance of the Cassini spacecraft from the center of Saturn. The small blue and red circles along this curve indicate the radial distances of the bow shock and the magnetopause, respectively, as determined in situ by Cassini. The shaded intervals indicate two occasions when there were many crossings of a boundary over a relatively short period; the small circles at the beginning and end of each interval indicate the observed radial distance for the boundary. These radial distances can be compared with the mSWiM propagation predictions, shown by the continuous lines. Figures 5c and 5d show the comparison before and after applying a shift of +1.9036 days to the propagations, respectively. (e) Product of the predicted SW density and velocity values (SW number flux) at Saturn (from Figure 1) after the +1.9 days shift. (f) Cassini RPWS time–frequency map. SKR frequencies range from ~800 kHz down to ~10 kHz, while narrow-band emissions are observed below 10 kHz. The SKR spectrum brightens from DOY 121 to 123, overlapping the second Chandra observation.

described here, will help to improve the predictive accuracy of the propagations.

4.2. Cassini Radio Data

[33] Data from Cassini RPWS (Radio and Plasma Wave Science; *Gurnett et al*., 2004) for the time interval of the Chandra observations are displayed in Figure 5f, in the form of a time spectrogram, where Saturn's kilometric radiation (SKR) ranges from 10 to 800 kHz. As at Earth, this intense nonthermal emission provides a powerful diagnostic of the Kronian auroral activity [e.g., *Kurth et al*., 2009, and references therein] as it is known to be produced on magnetic field lines with footprints in the auroral zone, by a population of accelerating electrons [*Lamy et al*., 2009] whose energies typically reach a few to a few tens of keV at the top of the atmosphere [*Gustin et al*., 2009]. Since Voyager times, it is well known that SKR activity is strongly controlled by the SW dynamic pressure [*Desch*, 1982; *Kurth et al*., 2005; *Rucker et al*., 2008; *Clarke et al*., 2009]. Therefore, continuous remote RPWS observations of SKR during the Chandra observations enabled us to monitor the aurora and check its response to the expected arrival of the interplanetary shocks at Saturn.

[34] Figure 5f shows an SKR intensification starting on DOY 121 and peaking on DOY 122. This appears to be consistent with what is revealed by our Cassini-mSWiM comparison: a compression of the magnetosphere occurred starting around DOY 120 (Figure 5d), with the Chandra observations on DOY 120 and 122 falling roughly around the start and the peak of the compression respectively. Inspection of the SW propagation profiles, after applying a shift by +1.9 days, shows the most significant forward shock occurring around DOY 122.5, with a pressure enhancement starting from DOY 120, i.e., roughly consistent with the SKR activity. In fact, because of propagation delays needed for the SW to enter the magnetosphere [e.g., *Clarke et al*., 2005] and force dawn auroral brightenings, necessarily SKR events will be late by at least a few hours with respect to timings determined in situ. Following a standard compression of the magnetosphere, the auroral oval is expected to broaden towards high latitudes and fill in the polar cap from midnight [*Prangé et al*., 2004; *Clarke et al*., 2005, 2009]. This structure then evolves in (sub-) corotation toward lower latitudes at noon. Given the spacecraft dusk location and the SKR anisotropic beam pattern [*Lamy et al*., 2008; *Cecconi et al*., 2009], it is possible that Cassini RPWS was able to observe the edges of the dawn side activated oval before the rotating bulk of the emission comes into view. Interestingly, narrow band emissions at ~5 kHz appear to intensify just before DOY 121. These emissions have been shown to be triggered by the SW [*Louarn et al*., 2007] and may relate to the compression of DOY 120.

[35] We can compare the case discussed above with the crossing of the first SKR source on DOY 291 of 2008, at high southern latitudes, close to midnight and at 5 R_S, which precisely followed a SW compression, revealing downward precipitating electrons with energies of 6–9 keV and upward travelling ions of more than 10 keV energy [*Bunce et al*., 2010; *Lamy et al*., 2010; *Schippers et al*., 2011]. This suggests that precipitating electrons may reach energies up to and above 20 keV. Although this corresponds to expected night-side precipitations for just one event, it still gives an order of magnitude estimate of the electron energies and a possible handle with which to determine the X-ray fluxes expected from electron bremsstrahlung.

[36] In Figure 5e, we note a major SW enhancement which took place during the day following the second Chandra observation and also the absence of predicted SW activity in correspondence of radio enhancements around DOY 117 and 126. While SKR emissions are strongly controlled by the SW, they are also sensitive to internal dynamics, which could explain the lack of correlation with SW conditions: for example, *Jackman et al*. [2009] identified a set of plasmoid ejections, which in turn triggered SKR enhancements, in phase with the planetary rotation.

5. Discussion

5.1. Saturnian X-ray Aurorae?

[37] The objective of our Chandra TOO observations of Saturn, scheduled to coincide with the predicted arrival of an interplanetary shock at the planet, was to maximize the chances of observing an X-ray auroral brightening. Although we did observe during an episode of enhanced compression by the SW at Saturn, we detected no auroral X-rays from CX or bremsstrahlung (with 3σ upper limits of 2 and 17 MW in the 0.3–2.0 keV and 2.0–8.0 keV bands, respectively). This compares with 0.2–2.0 keV upper limits in the range 8–24 MW derived for the CX component in previous observations of Saturn and of 94–147 MW for any bremsstrahlung emission in the range 2.0–8.0 keV [*BR10*; *Hui et al*., 2010b].

5.1.1. CX X-ray Aurora

[38] The lack of CX X-ray aurorae on Saturn has been discussed by *Hui et al*. [2010b] in an attempt to deduce what physical conditions may be responsible for it, at variance with the bright X-ray aurorae occurring on Jupiter. Based on the current knowledge of the emission mechanisms operating on Jupiter, *Hui et al*. considered SW and magnetospheric origins for the ions that could undergo CX, both in the presence and absence of local acceleration. In the particular case, relevant to our work, of SW ions, they use a mean value of 1.69×10^6 cm^{-2} s^{-1} for the SW number flux (density times flow speed), derived by averaging 19 days of measurements by Cassini immediately upstream of Saturn in January 2004; they also use an area for the cusps (where most of the ions are expected to precipitate) of 1.1×10^{19} cm^2, i.e., reaching down in latitude to 20^o from the pole (this is the region where the UV aurora is also confined, e.g., *Clarke et al*. [2009]; however, see also the study by *Bunce et al*. [2005] who estimate a typical cusp area of 10^{16} cm^2). The expected flux of auroral CX X-rays is only 0.5 MW, a factor of 4 lower than the upper limit set by the observations presented here. To raise this to a level close to detectability, following *Hui et al*. [2010b] we estimate that accelerating potentials of ~10 kV would be required (and are obviously not present). From Figure 1, we see that the enhanced SW number flux at the time of our Chandra observations was of the order of 5×10^6 cm^{-2} s^{-1}, i.e., three times higher than assumed by *Hui et al*., but still insufficient to generate an X-ray aurora by CX that could be detectable with Chandra. This suggests that much more dramatic episodes of solar wind enhancement than the one we have used as a trigger, and/or higher sensitivity of the observing facilities, would be needed to achieve a detection. We note that the alternative of CX on

magnetospheric ions (e.g., from Enceladus' plume) would require even higher potentials (8 MV, *Hui et al*., 2010b) in order for the ions to be stripped and raised to the H- and He-like states necessary for X-ray production.

5.1.2. X-ray Bremsstrahlung Aurora

[39] Taking a population of electrons of 10 keV energy (corresponding to a velocity of ~6×10^4 km s^{-1}) and assuming a density of 5×10^{-2} cm^{-3} (as measured by *Schippers et al*., 2011, for "hot" electrons at ~ 4 R_S during the 2008 SKR source crossing), we compute an electron energy flux of ~5×10^{-3} W m^{-2}. We follow *Gilman et al*. [1986], taking an aurora emission area of 4.9×10^{18} cm^2 (i.e., two auroral zones located between 78° and 81.5° in latitude), and calculate the input electron energy to be 2.3×10^{12} W, i.e., 19% of what *Gilman et al*. predict by extrapolating from the UV aurora, also assumed to originate from electron bremsstrahlung. For a power law electron energy distribution with index −3, the resulting bremsstrahlung X-ray spectrum at Earth is $I(E) = 4 \times 10^{-8} E^{-2}$ photons cm^{-2} s^{-1} keV^{-1}. Integrating between 2 and 8 keV gives an energy flux of 8.9×10^{-20} W m^{-2}, or ~1 MW for just one auroral zone, i.e., some 17 times lower than our Chandra upper limit (section 3.2). This very approximate calculation does not take into account the separate contributions of primary and secondary electrons and relies on density data far away from the surface of the planet (at ~4 R_S), but a similar result is obtained by using the canonical conversion rate of 10 kR of UV emission to a precipitating flux of ~1 mW m^{-2} [*Gérard and Sing*, 1982]. Given that Kronian UV aurorae typically produce 1–100 kR, we can expect electron energy fluxes of the order of 0.1–10 mW m^{-2}, again consistent with the Chandra upper limit.

[40] As an alternative, we could adopt a value for the electron density as measured at 1000 km; several authors [*Benson*, 1985; *Galopeau et al*., 1989; *Kliore et al*., 2009; *Fischer et al*., 2011a] report densities of the order of a few $\times 10^4$ cm^{-3} over the whole electron spectrum. For a power law distribution with index −3, extending from 0.1 to 10 keV, only a very small fraction (10^{-5}) of the particles would have energies on the order of 10 keV, leading to a predicted power still below the Chandra upper limit.

5.1.3. Solar Impact

[41] The spectrum from the first Chandra observation, when Saturn's disk was brighter, resembles very closely that of the active Sun (coronal emission with temperature of ~0.5 keV, plus significant Mg XI emission, typical of solar flares), suggesting that we are seeing solar X-rays scattered from the planet's atmosphere. Figure 6 shows a plot of the GOES solar X-ray flux at Earth, with the two black bars at the top indicating the Chandra observation times (with a light travel time difference of 2.4 hours added).

[42] The occurrence of bright solar flares that can be associated with the first observation suggests that the enhancement in Saturn's X-ray signal at that time is due to reflected solar X-rays, as in the first of the January 2004 Chandra observations reported by *Bhardwaj et al*. [2005a]. The decreased Mg XI emission in our second observation is consistent with this view. The degree of variability in 2011 (a decrease by ~30%, section 3.1) is smaller than that observed in 2004, when the visible part of the planet, unobscured by the rings, dimmed by a factor of more than 6 in countrate between two observations separated by a week. However, the disk total emitted power for each of our 2011 Chandra observations (Table 2) and the associated GOES X-ray fluxes (Figure 6) fit well the solar cycle–driven variability trend illustrated by *BR10* (their Figure 5).

5.2. Saturn's X-ray Line Emission and Ring X-rays

[43] The 2011 Chandra observations allow us to separate clearly the X-ray emissions of Saturn's disk and its rings: an emission line, of energy consistent with fluorescent OKα, is present in the spectrum of the rings but is missing from that of the disk. The line is clearly detected in both observations (Figure 4) and is possibly weaker in the second

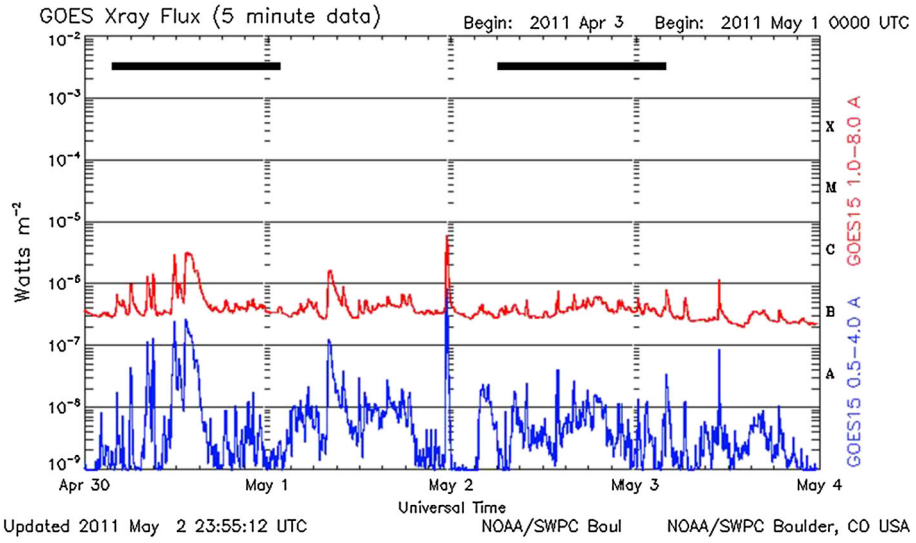

Figure 6. GOES-15 solar X-ray flux in the ranges 0.5–4.0 A (3–25 keV, blue) and 1.0–8.0 A (1.5–12.0 keV, red) around the time of the Chandra observations of Saturn. The two black bars at the top indicate the intervals corresponding to the Chandra observations (after correcting for the difference in the light travel time from the Sun to Saturn and to Earth and from the Sun to Earth).

(e.g., it is not present in the West ansa). One could speculate that this may be linked to the decay of the disk emission between the two observations and thus to a solar connection, but it would be at variance with the absence of such a correlation in earlier observations [*BR10*]. The power emitted in the line at its brightest (7 ± 4 MW) is more than a factor of 10 below the brightest measured by Chandra in 2004, 84 MW [*Bhardwaj et al*., 2005b], while the disk is only down by a factor of ~3. If there is a solar connection, this difference may be explained by the fact that, soon after Saturn's equinox (11 August 2009), the rings are close to side-on; the high inclination would make it more difficult to see any directly scattered X-rays from their surface, unless an optically thick, scattering atmosphere has a large scale height above and below the ring plane. However, typical scale heights are estimated to be 0.15 R_S for O_2^+ and substantially less for neutrals [*Johnson et al*., 2006].

[44] Saturnian thunderstorms are also expected to die down around the time of equinox, so the alternative suggestion invoking electron beams generated in the course of lightning strikes to excite the O emission cannot yet be excluded. We note, however, the earlier than expected emergence in the springtime season of a Great White Spot, a giant thunderstorm on Saturn's Northern hemisphere, in December 2010 [*Fischer et al*., 2011b]. On a separate note, this is unlikely to have a connection with the higher X-ray brightness of the North cap in our first Chandra observation (Table 1, section 3.1), given the scattering origin of the emission together with the slightly better visibility of the planet's Northern hemisphere at the time. Also, the lack of modulation of the X-ray flux at Saturn's rotation period argues against the presence of any effect due to the Great White Spot.

5.3. The Potential of Propagation Predictions

[45] In this paper, we report the first remote X-ray observations of a giant planet triggered on the basis of SW propagation predictions from near-Earth measurements. The SW propagations strongly suggest that the Chandra observations were made around the time of a SW compression of Saturn's magnetosphere, and Cassini in situ measurements confirm this. While we have not detected X-ray aurorae on Saturn, we have been successful in matching Cassini crossings of the planet's magnetospheric boundaries with predictions from the mSWiM propagation code and in pinpointing their timings precisely. A similar approach to triggering observations, in fact, an expansion of it to two planets, has subsequently been applied during the autumn of 2011 when Jupiter and Uranus, and also the Earth, were in opposition. A successful detection with the Hubble Space Telescope of UV aurorae on Uranus on that occasion has been reported by *Lamy et al.* [2012].

[46] Cassini, orbiting Saturn since 2004, has very significantly improved our understanding of Saturn's space environment. However, studies of Saturn's magnetosphere are limited by the absence of an additional spacecraft monitoring the state of the SW upstream of the planet. To address this, MHD simulations of SW evolution from Earth to Saturn, such as those provided by the mSWiM code, and their validation, are important contributors to studies of Saturn's magnetosphere. Moreover, they can tell us whether the model captures the physics of SW evolution and, if not, will point to the need of exploring why not. Opportunities to validate propagation predictions at Saturn will continue as long as Cassini operates and could be extended to the outer planets if space missions were to fly to them and make in situ measurements over long periods.

6. Conclusions

[47] The lack of detection of X-ray aurorae on Saturn at the time of a SW enhancement reaching the planet suggests that even stronger SW compression episodes are required to produce a signal detectable with the current Earth-bound X-ray observing facilities. An important difference with Jupiter, where bright X-ray aurorae are quite regularly observed, appears to be the lower accelerating potentials on Saturn, where 100 kV are expected to be required to produce SW CX emissions, and 8 MV for CX of magnetospheric ions, originating from Enceladus [*Hui et al*., 2010b]. While this is disappointing, similar repeated applications of SW propagation predictions could lead to improving their accuracy and to furthering the study of SW interactions with planetary bodies.

[48] In situ X-ray observations ought to be seriously considered as a possibility to enhance future planetary exploration probes, given the widespread detection of such high energy emissions in the solar system and the advantage in spatial, temporal, and spectral resolution they would afford. Short of this, more sensitive Earth-bound telescopes than those flying today are needed to take the Saturnian X-ray exploration further.

[49] **Acknowledgments.** We are grateful to Scott Wolk (CXO) for his invaluable assistance in setting up the Chandra observations, and to Deb Baker (UCL/MSSL) for her warning signals about solar activity. Cassini MAG and CAPS ELS science and operations were supported by UK STFC rolling grants to ICL and UCL and by ESA via the UK Space Agency. Support for PGF and GRG has come from SAO grant GO1-12181B. French coauthors acknowledge support from CNES (Centre National d'Etudes Spatiales), CNRS (Centre National de la Recherche Scientifique), and Observatoire de Paris. Planetary ephemerides used in this paper were provided by the Institute de Mécanique Céleste et de Calcul des Ephémérides (Observatoire de Paris, CNRS). We acknowledge the useful comments of two anonymous referees which have helped substantially to improve the paper.

References

Benson, R. F. (1985), Auroral kilometric radiation: Wave modes, harmonics, and source region electron density structures, *J. Geophys. Res.*, *90*, 2753–2784.

Bhardwaj, A., R. F. Elsner, J. H. Waite Jr., G. R. Gladstone, T. E. Cravens, and P. G. Ford (2005a), Chandra observation of an X-ray flare at Saturn: Evidence of direct solar control on Saturn's disk X-ray emissions, *Astrophys. J.*, *624*, L121–L124, doi:10.1086/430521.

Bhardwaj, A., R. F. Elsner, J. H. Waite Jr., G. R. Gladstone, T. E. Cravens, and P. G. Ford (2005b), The discovery of oxygen Kα X-ray emission from the rings of Saturn, *Astrophys. J.*, *627*, L73–L76, doi:10.1086/431933.

Bodewits, D., D. J. Christian, M. Torney, M. Dryer, C. M. Lisse, K. Dennerl, T. H. Zurbuchen, S. J. Wolk, A. G. G. M. Tielens, and R. Hoekstra (2007), Spectral analysis of the Chandra comet survey, *Astron. Astrophys.*, *469*, 1183–1195.

Branduardi-Raymont, G., A. Bhardwaj, R. F. Elsner, G. R. Gladstone, G. Ramsay, P. Rodriguez, R. Soria, J. H. Waite Jr., and T. E. Cravens (2007), A study of Jupiter's aurorae with XMM-Newton, *Astron. Astrophys.*, *463*, 761–774, doi:10.1051/0004-6361:20066406.

Branduardi-Raymont, G., A. Bhardwaj, R. F. Elsner, and P. Rodriguez (2010), X-rays from Saturn: a study with XMM-Newton and Chandra over the years 2002–05, *Astron. Astrophys.*, *510*, 73–81, doi:10.1051/0004-6361/200913110 [*BR10*].

Bunce, E. J., S. W. H. Cowley, and S. E. Milan (2005), Interplanetary magnetic field control of Saturn's polar cusp aurora, *Ann. Geophys.*, *23*, 1405–1431.

Bunce, E. J., S. W. H. Cowley, D. L. Talboys, M. K. Dougherty, L. Lamy, W. S. Kurth, P. Schippers, B. Cecconi, P. Zarka, C. S. Arridge, et al. (2010), Extraordinary field-aligned current signatures in Saturn's high-

latitude magnetosphere: Analysis of Cassini data during Revolution 89, *J. Geophys. Res.*, *115*, A10238, doi:10.1029/2010JA015612.

Cecconi, B., L. Lamy, P. Zarka, R. Prangé, W. S. Kurth, and P. Louarn (2009), Goniopolarimetric study of the revolution 29 perikrone using the Cassini Radio and Plasma Wave Science instrument high-frequency radio receiver, *J. Geophys. Res.*, *114*, A03215, doi:10.1029/2008JA013830.

Christian, D. J., D. Bodewits, C. M. Lisse, K. Dennerl, S. J. Wolk, H. Hsieh, T. H. Zurbuchen, and L. Zhao (2010), Chandra observation of comets 8P/Tuttle and 17/P and 17P/Holmes during solar, *Ap. J. Supp. Series*, *187*, (2), 447–459.

Clarke, J. T., J.-C. Gérard, D. Grodent, S. Wannawichian, J. Gustin, J. Connerney, F. Crary, M. Dougherty, W. Kurth, S. W. H. Cowley, et al. (2005), Morphological differences between Saturn's ultraviolet aurorae and those of Earth and Jupiter, *Nature*, *433*, 717–719.

Clarke, J. T., J. Nichols, J.-C. Gérard, D. Grodent, K. C. Hansen, and another 16 co-authors (2009), Response of Jupiter's and Saturn's auroral activity to the solar wind, *J. Geophys. Res.*, *114*, A05210, doi:10.1029/2008JA013694.

Cravens, T. E. (1997), Comet Hyakutake x-ray source: Charge transfer of solar wind heavy ions, *Geophys. Res. Lett.*, *24*, 105–108.

Cravens, T. E. (2000), Heliospheric X-ray emission associated with charge transfer of the solar wind with interstellar neutrals, *Astrophys. J.*, *532*, L153–L156.

Dennerl, K. (2010), Charge transfer reactions, *Space Sci. Rev.*, *157*, 57–91, doi:10.1007/s11214-010-9720-5.

Desch, M. D. (1982), Evidence for solar wind control of Saturn radio emission, *J. Geophys. Res.*, *87*, 4549–4554.

Dougherty, M. K., et al. (2004), The Cassini magnetic field investigation, *Space Sci. Rev.*, *114*, 331–383, doi:10.1007/s11214-004-1432-2.

Fischer, G., D. A. Gurnett, W. S. Kurth, F. Akalin, P. Zarka, U. A. Dyudina, W. M. Farrell, and M. L. Kaiser (2008), Atmospheric electricity at Saturn, *Space Sci. Rev.*, *137*, 271–285, doi:10.1007/s11214-008-9370-z .

Fischer, G., D. A. Gurnett, P. Zarka, L. Moore, and U. A. Dyudina (2011a), Peak electron densities in Saturn's ionosphere derived from the low-frequency cutoff of Saturn lightning, *J. Geophys. Res.*, *116*, A04315, doi:10.1029/2010JA016187.

Fischer, G., et al. (2011b), A giant thunderstorm on Saturn, *Nature*, *475*, 75–77, doi: 10.1038/nature10205.

Ford, P. G., and R. E. Elsner (2005), X-ray spectroscopy of optically bright planets with the Chandra observatory, *AGU*, P44A–06.

Galopeau, P., P. Zarka, and D. Le Queau (1989), Theoretical model of Saturn's Kilometric Radiation spectrum, *J. Geophys. Res.*, *94*, 8739–8755.

Gérard, J.-C., and V. Sing (1982), A Model of energy deposition of energetic electrons and EUV emission in the Jovian and Saturnian atmospheres and implications, *J. Geophys. Res.*, *87*, 4525–4532.

Gilman, D. A., K. C. Hurley, F. D. Seward, H. W. Schnopper, J. D. Sullivan, and A. E. Metzger (1986), An upper limit to X-ray emission from Saturn, *Astrophys. J.*, *300*, 453–455.

Gurnett, D. A., W. S. Kurth, D. L. Kirchner, G. B. Hospodarsky, T. F. Averkamp, P. Zarka, and another 24 co-authors (2004), The Cassini radio and plasma wave investigation, *Space Sci. Rev.*, *114*, 395–463, doi:10.1007/s11214-004-1434-0.

Gustin, J., J.-C. Gérard, W. Pryor, P. D. Feldman, D. Grodent, and G. Holsclaw (2009), Characteristics of Saturn's polar atmosphere and auroral electrons derived from HST/STIS, *FUSE and Cassini/UVIS spectra, Icarus*, *200*, 176–187, doi:10.1016/j.icarus.2008.11.013.

Hui, Y., D. R. Schultz, V. A. Kharchenko, A. Bhardwaj, G. Branduardi-Raymont, P. C. Stancil, T. E. Cravens, C. M. Lisse, and A. Dalgarno (2010a), Comparative analysis and variability of the Jovian X-ray spectra detected by the Chandra and XMM-Newton observatories, *J. Geophys. Res.*, *115*, A07102, doi:10.1029/2009JA014854.

Hui, Y., T. E. Cravens, N. Ozak, and D. R. Schultz (2010b), What can be learned from the absence of auroral X-ray emission from Saturn?, *J. Geophys. Res.*, *115*, A10239, doi:10.1029/2010JA015639.

Jackman, C. M., L. Lamy, M. P. Freeman, P. Zarka, B. Cecconi, W. S. Kurth, S. W. H. Cowley, M. K. Dougherty (2009), On the character and distribution of lower-frequency radio emissions at Saturn and their relationship to substorm-like events, *J. Geophys. Res.*, *114*, A08211, doi:10.1029/2008JA013997.

Johnson, R. E., J. G. Luhmann, R. L. Tokar, M. Bouhram, J. J. Berthelier, E. C. Sittler, J. F. Cooper, T. W. Hill, H. T. Smith, M. Michael, et al. (2006), Production, ionization and redistribution of O_2 in Saturn's ring atmosphere, *Icarus*, *180*, 393–402, doi:10.1016/j.icarus.2005.08.021.

Kanani, S. J., C. S. Arridge, G. H. Jones, A. N. Fazakerley, H. J. McAndrews, N. Sergis, and another 6 co-authors (2010), A new form of Saturn's magnetopause using a dynamic pressure balance model, based on *in situ*, multi-instrument Cassini measurements, *J. Geophys. Res.*, *115*, A06207, doi:10.1029/2009JA014262.

Kliore, A. J., A. F. Nagy, E. A. Marouf, A. Anabtawi, E. Barbinis, D. U. Fleischman, and D. S. Kahan (2009), Mid-latitude and high-latitude electron density profiles in the ionosphere of Saturn obtained by Cassini radio occultation observations, *J. Geophys. Res.*, *114*, A04315, doi:10.1029/2008JA013900.

Kurth, W. S., D. A. Gurnett, J. T. Clarke, P. Zarka, M. D. Desch, M. L. Kaiser, and another 9 co-authors (2005), An Earth-like correspondence between Saturn's auroral features and radio emission, *Nature*, *433*, 722–725, doi:10.1038/nature03334.

Kurth, W. S., E. J. Bunce, J. T. Clarke, F. J. Crary, D. C. Grodent, A. P. Ingersoll, and another 7 co-authors (2009), Auroral Processes, Saturn from Cassini-Huygens, 333–374. Ed.s M. K. Dougherty, L. W. Esposito, S. M. Krimigis. Springer Science+Business Media, The Netherlands, doi: 10.1007/978-1-4020-9217-6_12.

Lamy, L., P. Zarka, B. Cecconi, S. Hess, and R. Prangé (2008), Modeling of Saturn kilometric radiation arcs and equatorial shadow zone, *J. Geophys. Res.*, *113*, A10213, doi:10.1029/2008JA013464.

Lamy, L., B. Cecconi, R. Prangé, P. Zarka, J. D. Nichols, and J. T. Clarke (2009), An auroral oval at the footprint of Saturn's kilometric radio sources, colocated with the UV aurorae, *J. Geophys. Res.*, *114*, A10212, doi:10.1029/2009JA014401.

Lamy, L., P. Schippers, P. Zarka, B. Cecconi, C. S. Arridge, M. K. Dougherty, and another 6 co-authors (2010), Properties of Saturn kilometric radiation measured within its source region, *Geophys. Res. Lett.*, *37*, L12104, doi: 10.1029/2010GL043415.

Lamy, L., R. Prangé, K. C. Hansen, J. T. Clarke, P. Zarka, B. Cecconi, and another 13 authors (2012), Earth-based detection of Uranus' aurorae, *Geophys. Res. Lett.*, *39*, L07105, doi:10.1029/2012GL051312.

Linder, D. R, A. J. Coates, R. D. Woodliffe, C. Alsop, A. D. Johnstone, M. Grande, A. Preece, B. Narheim, and D. T. Young (1998), The Cassini CAPS electron spectrometer, in *Measurement Techniques for Space Plasmas: Particles*, *Geophys. Monogr. Ser.*, *102*, 257–262, edited by R. F. Pfaff, J. E. Borovsky, and D. T. Young, American Geophysical Union, Washington DC.

Louarn, P., W. S. Kurth, D. A. Gurnett, G. B. Hospodarsky, A. M. Persoon, B. Cecconi, and another 10 co-authors (2007), Observation of similar radio signatures at Saturn and Jupiter: Implications for the magnetospheric dynamics, *Geophys. Res. Lett.*, *34*, L14108–L14114, doi:10.1029/2007GL030368.

Ness, J.-U., J. H. M. M. Schmitt, and J. Robrade (2004a), Detection of Saturnian X-ray emission with XMM-Newton, *Astron. Astrophys.*, *414*, L49–L52.

Ness, J.-U., J. H. M.M. Schmitt, S. J. Wolk, K. Dennerl, and V. Burwitz (2004b), X-ray emission from Saturn, *Astron. Astrophys.*, *418*, 337–345, doi:10.1051/0004-6361:20035736.

Prangé, R., L. Pallier, K. C. Hansen, R. Howard, A. Vourlidas, R. Courtin, and C. Parkinson (2004), An interplanetary shock traced by planetary auroral storms from the Sun to Saturn, *Nature*, *432*, 78–81, doi:10.1038/nature02986.

Pryor W. R., A. M. Rymer, D. G. Mitchell, T. W. Hill, D. T. Young, and another 24 co-authors (2011), The auroral footprint of Enceladus on Saturn, *Nature*, *472*, 331–333, doi:10.1038/nature09928.

Rucker, H. O., et al. (2008), Saturn kilometric radiation as a monitor for the solar wind? *Adv. Space Res.*, *42*, 40–47, doi:10.1016/j.asr.2008.02.008.

Schippers, P., C. S. Arridge, J. D. Menietti, D. A. Gurnett, L. Lamy, B. Cecconi, and another 8 co-authors (2011), Auroral electron distributions within and close to the Saturn kilometric radiation source region, *J. Geophys. Res.*, *116*, A05203, doi:10.1029/2011JA016461.

Stallard, T., H. Melin, S. W. H. Cowley, S. Miller, and M. B. Lystrup (2010), Location and magnetospheric mapping of Saturn's mid-latitude infrared auroral oval, *Astrophys. J. Lett.*, *722*, L85–L89, doi:10.1088/2041-8205/722/1/L85.

Went, D. R., G. B. Hospodarsky, A. Masters, K. C. Hansen, and M. K. Dougherty (2011), A new semiempirical model of Saturn's bow shock based on propagated solar wind parameters, *J. Geophys. Res.*, *116*, A07202, doi:10.1029/2010JA016349.

Young, D. T., J. J. Berthelier, M. Blanc, J. L. Burch, A. J. Coates, R. Goldstein, M. Grande, T. W. Hill, and another 50 co-authors (2004), Cassini Plasma Spectrometer investigation, *Space Sci. Rev.*, *114*, 1–112, doi:10.1007/s11214-004-1406-4.

Zieger, B., and K. C. Hansen (2008), Statistical validation of a solar wind propagation model from 1 to 10 AU, *J. Geophys. Res.*, *113*, A08107, doi:10.1029/2008JA013046.